# Conversion of Liquids to Cluster Beams by Adiabatic Expansion of Liquid Jets: Mass Spectrometric Analysis of Molecular Association in Aqueous Solution Systems

**Nobuyuki Nishi* and Kazunori Yamamoto**

*Contribution from the Institute for Molecular Science, Myodaiji-cho, Okazaki 444, Japan.*
*Received May 8, 1987*

**Abstract:** Stability of hydrate clusters in aqueous solution has been studied by means of mass spectrometry of cluster beams generated through the adiabatic expansion of a liquid jet. Details of the beam generator and some characterizations are reported. Stability constants of $\kappa_1$ and $\kappa_2$ for solute monomer hydrates and dimer hydrates, respectively, are defined in relation to the equilibrium constants for molecular exchange processes of the clusters in liquids. Among 13 solute species investigated, the order of stability (or rigidness) of the monomer hydrates is carboxylic acids > alcohols > amides ≥ amines > acetone ≫ acetonitrile. That of the dimer hydrates relative to the respective monomer hydrates is carboxylic acids ≳ alcohols > amides ≳ amines. These constants changed even among the same group of solute species sensitively due to the substituent(s). Van't Hoff plots of the ion intensity ratios provided the enthalpy changes for the differential molecular processes in solution. In the ethanol–water (1:100) system, strong evidence of alcohol–alcohol association was found and its origin was attributed to hydrophobic hydration of ethyl groups in an aqueous environment. Stabilization energy for the exchange process $(C_2H_5OH)_m(H_2O)_n + C_2H_5OH \rightarrow (C_2H_5OH)_{m+1}(H_2O)_{n-1} + H_2O$ was obtained to be 4.5 (±0.6) kcal/mol for $0 \le m \le 2$ and $11 - m \le n \le 15 - m$, although the measured values increased slightly for larger values of $m$.

## I. Introduction

The "flickering cluster" model, proposed by Frank and Wen[1] and by Némethy and Scheraga,[2] has been shown to describe various properties of liquids very well.[1-4] Hydrogen bond formation of water molecules in aqueous solutions is thought to form clusters with "ice-like" structure that are stabilized by the presence of a hydrophobic group.[4,5] On the basis of a quantitative assessment of the hydrophobic effect from the standard free energy, enthalpy, and entropy of solution of a large number of gaseous nonpolar nonelectrolytes, Abraham concluded that the hydrophobic effect of a methylene group in *n*-alkanes is primarily an enthalpic effect that arises through a methylene/water interaction.[6] On the other hand, polar solute species with hydrogen bonding ability are also expected to show enthalpy changes for solvation in water. Recent Monte Carlo calculations on the hydration of methanol in an infinitely dilute aqueous solution showed that the hydrophobic region is characterized by large overall energy stabilization as a result of the sum of a large number of smaller interactions.[7] The relation $|\Delta H^E| < T|\Delta S^E|$ has been labeled as "typically aqueous" by Rowlinson[8] and Franks[4] for nonelectrolyte solute molecules. How does the association of solute species change the stability of water clusters? Solutions containing solute species with molar fractions in the region of 0.005–0.05 are of particular interest in this connection.

The understanding of the chemistry of aqueous solutions in terms of "fragments" is highly necessary for analyzing the real situation since measurement of overall average properties of a solution does not provide realistic information on the local structure.

Simple adiabatic expansion of a drop of liquid in vacuum causes instantaneous fragmentation by dissociating molecules that are weakly bound to hydrogen-bonded clusters through van der Waals forces. Evaporation of weakly bound molecules also cools the clusters by the transfer of internal energy to kinetic energy. In the expansion process, the relative distances between molecules and clusters gets longer very quickly. For a flight distance of 100 Å (which is almost interaction-free length for neutral species), one could estimate the flight time of a water molecule at 360 K to be about $10^{-11}$ s by assuming a translational energy of $kT$. Here, we report the development of a new molecular beam technique based on this principle and used for the conversion of a liquid to clusters of its "fragments". Mass spectrometry was applied for the detection of the cluster beams. Although electron impact ionization dissociates the parent clusters to some extent, the detected ions are still "fragments" of the liquid.

Quantitative analysis of the ion intensity ratios has been shown to throw light on the stability of hydrate clusters. Temperature change experiments provided information on the enthalpy changes involved in differential molecular processes of clusters such as molecular exchange, dissociation, and attachment "reactions".

## II. Experimental Section

The main part of the beam generator is shown in Figure 1. The nozzle was changed from the previous version reported.[9] The most important change is the use of commercial syringe needles as the liquid and gas nozzles. A Hamilton syringe needle of inner diameter 0.13 mm and outer diameter 0.25 mm (type N731) was used as the liquid nozzle. One end of the needle was inserted into a stainless steel pipe with an inner diameter of 0.3 mm and fixed in it with "Torr Seal" epoxy resin. Another syringe needle (Hamilton type N724) was used as a gas nozzle in which the liquid-nozzle needle was inserted. The head of the gas nozzle is situated about 0.3 mm behind the end of the liquid nozzle. Stagnation pressure of argon in the gas nozzle was in the range of 20–100 Torr. Higher pressure caused strong interaction between the liquid jet and gas flow resulting in instability of the beam. One can produce cluster beams even without flowing gas, but they are sometimes unstable. The temperature of the needle was measured at a position 4 mm behind the liquid-nozzle head with a copper–constantan thermocouple. The stainless steel liquid pipe was indirectly heated through the gas pipe and the pipe holder. The temperature of the gas pipe in contact with Thermocoax heating elements was monitored by another copper–constantan thermocouple. The vacuum in the expansion chamber was maintained below 0.3 Torr and that of the detection chamber was lower than $1 \times 10^{-7}$ Torr. The pressure of the flowing liquid in the stainless steel pipe was measured by a Bourdon type pressure gage (Shinagawa Sokki, Model LCG50D) directly connected to the pipe at the entrance to the vacuum chamber. Other experimental conditions were the same as described in the previous paper.[9] The change of nozzle greatly improved the stability of the cluster beams and hence expanded the measurable temperature range of the liquid.

(1) Frank, H. S.; Wen, W.-Y. *Discuss. Faraday Soc.* **1957**, *24*, 133.
(2) Némethy, G.; Scheraga, H. A. *J. Chem. Phys.* **1962**, *36*, 3382.
(3) Marcus, Y. *Introduction to Liquid State Chemistry*; J. Wiley: Chichester, 1977; Chapter 3, Section 2.
(4) (a) Franks, F. In *Water: A Comprehensive Treatise*; Plenum: New York, 1973; Vol. 2, Chapter 1. (b) Franks, F.; Reid, D. S. *Ibid.*, Chapter 5.
(5) Frank, H. S.; Evans, M. W. *J. Chem. Phys.* **1945**, *13*, 507.
(6) Abraham, M. H. *J. Am. Chem. Soc.* **1982**, *104*, 2085.
(7) Okazaki, S.; Nakanishi, K.; Touhara, H. *J. Chem. Phys.* **1983**, *78*, 454.
(8) Rowlinson, J. S. In *Liquids and Liquid Mixtures*, 2nd ed.; Butterworths: London, 1969.
(9) Nishi, N.; Yamamoto, K.; Shinohara, H.; Nagashima, U.; Okuyama, T. *Chem. Phys. Lett.* **1985**, *122*, 599.

0002-7863/87/1509-7353$01.50/0 

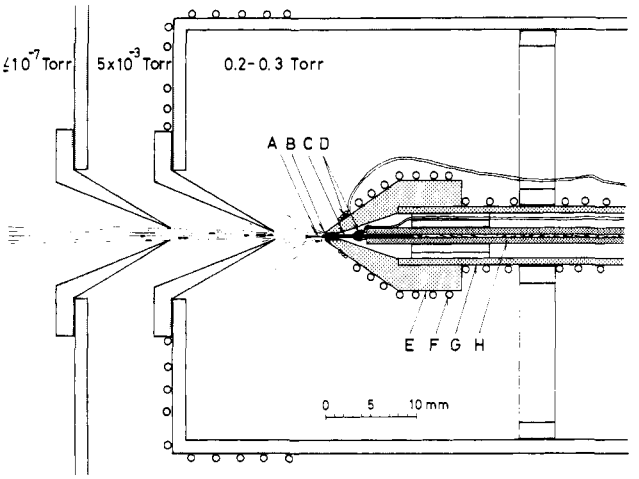


**Figure 1.** Beam generator for the conversion of liquids to cluster beams: A, liquid jet; B, nozzle head surrounded by a cylindrical gas nozzle (o.d. = 0.30 mm, i.d. = 0.25 mm); C, syringe needle (Hamilton N731; o.d. = 0.25 mm, i.d. = 0.13 mm); D, copper–constantan thermocouple; E, gas nozzle cap; F, flexible heater element; G, $^1/_4$-in. stainless steel pipe; H, $^1/_{16}$-in. stainless steel pipe (i.d. = 0.30 mm). The nozzle–skimmer distance was set to 2.5 mm in the present study.

The clusters were ionized by electron impact at 40 eV. The ionizer was situated at 8 cm downstream from the nozzle. The ions were directed at 90° to the beam direction and were analyzed by a quardupole mass spectrometer (ANELVA AGA-360). Signals from a ceramic electron multiplier (Murata EMS-6081B) were amplified by an electrometer and averaged for 128 scans, using a Nicolet 1170 signal averager with 4096 data points.

Ion transmission of a quadrupole mass filter and sensitivity of a secondary electron multiplier are dependent on the mass number of ions. Therefore, for the comparison of relative intensities it is necessary to correct for the mass dependence of ion sensitivity. This correction was made by comparing the intensity distribution of perfluoro-*n*-hexane with that taken by a double-focus electrostatic-magnetic spectrometer (JEOL JMS D300). For mass numbers larger than 60 and smaller than or equal to 200, the sensitivity change was found to be expressed by the formula

$$I(m) = Am^{-1/2}\exp(-\alpha m)$$

and for mass numbers larger than 200, the following equation fits to the observed sensitivity change

$$I(m) = B\exp(-\beta m)$$

where $m$ represents the mass number. Typical values of the constants $\alpha$, $\beta$, and $B/A$ were 0.0095, 0.0057, and 30.36, respectively. Whenever a filament of the ionizer was changed or any adjustment of the spectrometer was performed, the sensitivity was re-calibrated.

Liquid-chromatograph grade water, ethanol, and isopropyl alcohol were used without further purification. Other solute reagents were Tokyo Kasei's guaranteed grade and did not contain any serious impurity according to specifications. For the measurement of ethylamine and formamide solutions, deuteriated water (Aldrich gold label, 99.8%) was used as a solvent.

**Characterization of the Beams.** In order to examine the character of the cluster beams, the mass spectra of beams generated from pure water and aqueous ethanol solution were measured while the following parameters were changed: (1) flow rate of liquid, (2) gas stagnation pressure in the gas nozzle, (3) nozzle–skimmer distance, and (4) nozzle temperature. Also (5) the temperature of the expanding liquid was calibrated by observing the phase separation temperatures of 2-butoxyethanol aqueous solution.

**(1) Flow Rate of Liquid.** Generation of a liquid jet from the nozzle required pressurization of the liquid. For the expansion of water, the minimum flow rate was about 0.05 mL/min. Increase of the flow rate to larger than 0.2 mL/min made the jet flow unstable. This range of stable beam generation changed and was dependent upon the solute concentration. Aqueous ethanol solution produced highly stable cluster beams even at a flow rate of 0.3 mL/min. In the range of 0.08–0.2 mL/min, no spectral change was seen as long as the temperature was maintained constant. This fact indicates that the increase of the beam density by 2.5 times does not seriously cause collision-induced destruction of clusters in the expanding region. A flow rate of 0.1 mL/min was adopted in most cases.

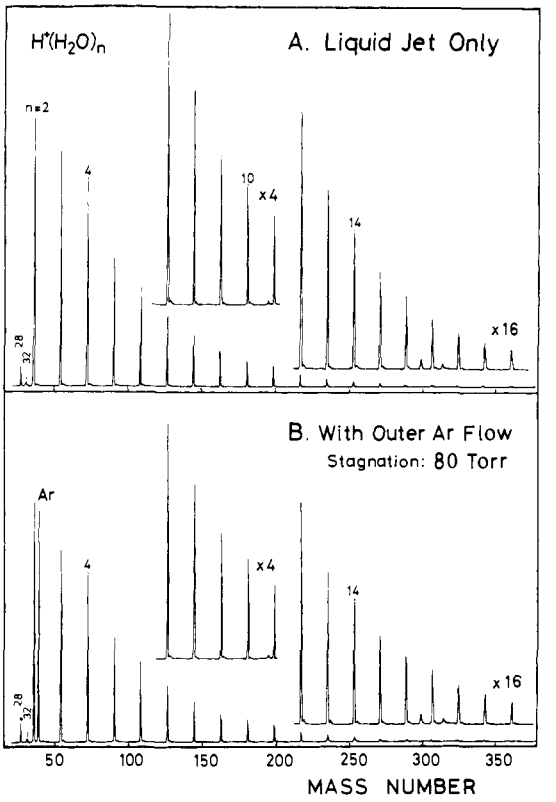


**Figure 2.** Mass spectra of water clusters generated from liquid water at 90 °C; (top) without flowing outer gas, (bottom) with Ar gas flow from a cylindrical gas nozzle at a stagnation pressure of 80 Torr.

**(2) Gas Stagnation Pressure.** The presence of the outer gas flow is indispensable to the generation of a stable cluster beam at low temperatures. Adequate stagnation pressure was dependent on the conductance of the cylindrical gap between the liquid nozzle and the inner surface of the gas nozzle. For the present dimensions, the stagnation pressure was maintained within a range of 20–100 Torr. No change of the spectral pattern was seen in this pressure range. This is also consistent with the result that an increase in the flow rate of the liquid jet did not change the spectral pattern within a range of 0.08–0.2 mL/min. Under the present conditions, collisional destruction of the clusters did not provide appreciable contribution to the cluster distributions. Figure 2 shows the mass spectra of the clusters produced from neat water at 90 °C. The top spectra was taken without flowing outer Ar gas. The bottom one was observed by flowing Ar gas at a stagnation pressure of 80 Torr. One can see the intensity of Ar at mass 40 is comparable to that of $H^+(H_2O)_2$ and ten times as strong as that of $N_2$ in the background. Although larger cluster intensities did not change appreciably on the introduction of Ar gas, smaller cluster intensities decreased slightly probably due to the collisional effect. However, the amount of the intensity decrease of $H^+(H_2O)_2$ is only 10% under the present condition. Collisional destruction of clusters was observed when the pressure of the expansion chamber was increased to greater than 1 Torr by reducing the pumping speed of the chamber.

**(3) Nozzle–Skimmer Distance.** The position of the first skimmer affects the relative intensities of high mass clusters. Figure 3 shows intensity changes of $H^+(H_2O)_3$, $H^+(H_2O)_{11}$, and $H^+(H_2O)_{20}$ signals as a function of nozzle–skimmer distance. Location of the skimmer at a long distance eliminated the relative contribution of smaller clusters, although all signals decreased. This result indicates that the divergence angles of the small clusters are relatively much wider and collisional destruction of the clusters becomes more serious for larger nozzle–skimmer distance. It is necessary to keep the distance shorter than 3 mm in order to avoid the contribution of the collisional effect in the spectral pattern. On the other hand, one can strip the solvent molecules off with the positive aid of the collision leaving the solute complexes existing in the core of clusters. This is collisional desolvation and will be reported for more complicated systems.

**(4) Nozzle Temperature.** The temperature 4 mm behind the end of the liquid nozzle was always monitored during the measurements. Actual temperature at the top of the liquid nozzle was thought to be lower than that at the sensor position because of the cooling due to evaporation of the molecules in the interface region. Since a flow rate of 0.1 mL/min

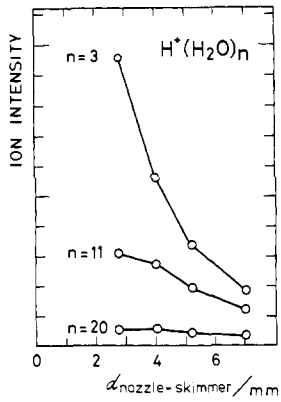


**Figure 3.** Intensity changes of the cluster ions, $H^+(H_2O)_3$, $H^+(H_2O)_{11}$, and $H^+(H_2O)_{20}$, as a function of nozzle–skimmer distance.

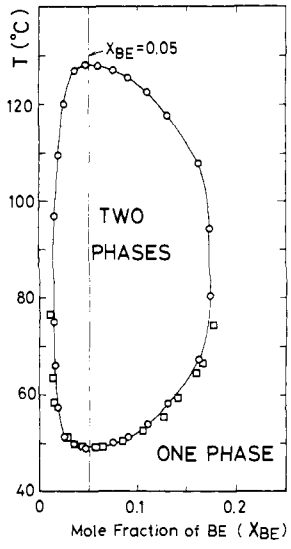


**Figure 4.** Miscibility curve of 2-butoxyethanol (BE) and water mixture: (○) from ref 10, (□) from ref 11.

produces a liquid stream at a velocity of 20 cm/s in the needle, the temperature of the liquid jet was expected to be close to the nozzle temperature. This nozzle temperature, however, was also affected by the thermal radiation from the surrounding gas-nozzle wall. This may cause a temperature gradient between the outer surface and the inner surface of the needle since the liquid is flowing. Solutions with more than 10% of methanol or ethanol produced stable beams at relatively lower temperatures compared to pure water which required a nozzle temperature higher than 70 °C. Nozzle temperatures higher than 200 °C did not give spectra appropriate to the temperature change suggesting that the liquid was not so hot as the needle. This must be due to the fast flow rate. Even at lower temperatures, it required 30 min or more after changing the heater voltage to get the spectral pattern constant.

**(5) Calibration of Liquid Temperature.** Direct measurement of the temperature of the liquid jet is a fairly difficult problem. Molecular composition of the cluster beams must depend on the liquid temperature just before the expansion since the expansion process is an instantaneous cooling or freezing process that cannot provide any energy for the change of the molecular configuration. How can we know the temperature of the liquid in which the final molecular configuration is originated? The method we adopted is the observation of the lower critical solution temperature (LCST) and the upper critical solution temperature (UCST) of the binary solution of 2-butoxyethanol (BE) that shows phase separation in the temperature range between the two critical temperatures.

Figure 4 shows the miscibility curve of BE aqueous solution observed by Cox and Cretcher[10] and Ito et al.[11] For the binary solution with $x_{BE}$(mole fraction of 2-butoxyethanol) = 0.05, the UCST and the LCST appear at 128 and 49 °C, respectively. In the two-phase region, this solution produces a large amount of water-rich portions and a small amount of water-poor portions. Thus, the intensities of pure solute clusters relative to those of hydrated species are expected to decrease on the decremental change of the temperature from the high-temperature one-phase region to the two-phase region.

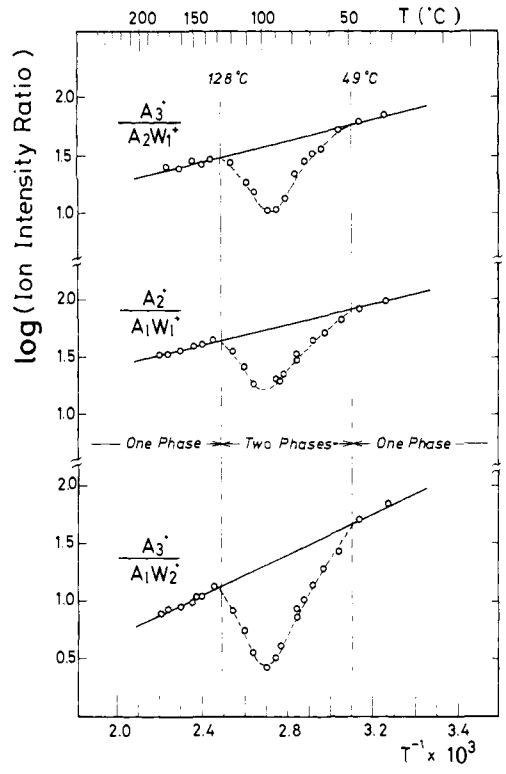


**Figure 5.** Logarithmic plots of intensity ratios $[H^+(BE)_3]/[H^+(BE)_2(H_2O)]$ ($\equiv A_3/A_2W$), $[H^+(BE)_2]/[H^+(BE)(H_2)]$ ($\equiv A_2/AW$), and $[H^+(BE)_3]/[H^+(BE)(H_2O)_2]$ ($\equiv A_3/AW_2$) against $1/T$ observed for a BE–water solution with a mole fraction of BE of 0.05. In the two-phase region between 128 and 49 °C, water-rich clusters increase because of the higher abundance of water-rich portion as expected from Figure 4.

Figure 5 shows the logarithmic plots of the intensity ratios $[H^+(BE)_3]/[H^+(BE)_2(H_2O)]$ ($\equiv A_3/A_2W$), $[H^+(BE)_2]/[H^+(BE)(H_2O)]$ ($= A_2/AW$), and $[H^+(BE)_3]/[H^+(BE)(H_2O)_2]$ ($\equiv A_3/AW_2$) against the inverse of absolute temperature ($1/T$). As elucidated in a later section, these plots for an one-phase solution are expected to show linear changes of which slopes are related to the enthalpy changes of the relevant molecular exchange processes in the solution. In the two-phase region, these intensity ratios change due to the contribution of the major water-rich phase. Actually the observed ratios decreased suddenly after passing the UCST point at 128 °C and again began to increase at 95 °C approaching to the values linearly extrapolated from the plots in the high-temperature (one-phase) region. The temperature difference between the two crossing points was 79 ± 6 °C which actually corresponds to the difference between the UCST and the LCST points. The UCST point was observed at a liquid–nozzle temperature of 168 ± 3 °C and the LCST was seen at a nozzle temperature of 89 ± 3 °C. Thus the nozzle temperature was found to be 40 ± 3 °C higher than the temperature of the expanding liquid jet.

## III. Results and Discussion

**Cluster Size Distribution of the Beams Produced from Pure Water.** For diagnosis of the cluster-beam character, the mass spectral distribution of pure water clusters was examined before the measurement of binary solutions. Figure 6 shows the corrected ion intensity distribution of water clusters. The distribution changed with the temperature of the liquid. At temperatures lower than 55 °C, the size of the most abundant water clusters was larger than water 20-mer. When the temperature was cooled to lower than 30 °C, the beam became very unstable and disappeared from the axis. The periodic bursting of the nozzle–chamber pressure suggested occasional trickling of the liquid due to the increase of the viscosity at lower temperatures.

As stated below, water clusters are thought to loose 1–3 water molecules on the electron impact ionization. Therefore, the parent species of the fragment ions are larger than the observed numbers.

(10) Cox, H. L.; Cretcher, L. H. *J. Am. Chem. Soc.* **1926**, *48*, 451.
(11) Ito, N.; Fujiyama, T.; Udagawa, Y. *Bull. Chem. Soc. Jpn.* **1983**, *56*, 379.

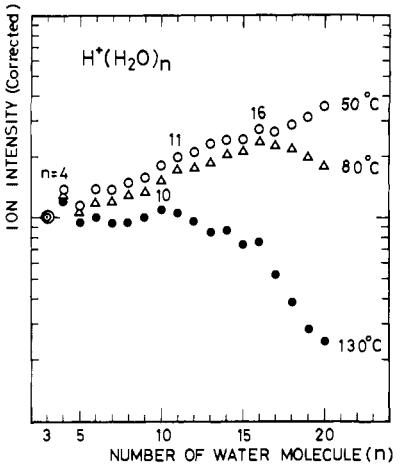


Figure 6. Cluster ion distribution of pure water at temperatures of 50, and 130 °C. Ionization electron energy = 40 eV. The sensitivity of the detector system was corrected for mass numbers.

De Raedt et al. performed a molecular dynamic calculation of 63 water molecules including a muonium and found that the average coordination numbers of water are 18 and 23.[12] Although the largest measured cluster is $H^+(H_2O)_{20}$, the cluster distribution of 50 °C water (at a pressure of 3.0 bar) seems to have a peak for 20–25-mer judging from the distribution of water clusters at 80 °C. In all three distributions, a peak or a hump was seen around 16-mer and this may arise mainly from the parent clusters with 18 molecules. At 120 °C, a peak was seen at water 10-mer indicating the presence of stable $(H_2O)_{11}$ and/or $(H_2O)_{12}$. This distribution is analogous to that of the cluster beam produced by supersonic expansion of gaseous water at a stagnation pressure of 307 Torr[13] except for the rather rapid drop at $n > 17$ in the liquid beam distribution. Hermann et al. reported the presence of the stable $(H_2O)_{11}$ and $(H_2O)_{12}$ species based on logarithmic derivative curves of intensity versus cluster size for various stagnation conditions.[13] However, the distribution at 50 and 80 °C in Figure 6 does not show any prominent hump around water 10-mer.

**Mass Spectra of Cluster Beams Generated from Binary Solutions.** Binary aqueous solutions of 13 solute species (methanol, ethanol, isopropyl alcohol, ethylene glycol, formic acid, acetic acid, methylamine, ethylamine, formamide, *N*-methylformamide, *N*-methylacetoamide, acetonitrile, and acetone) were expanded in a vacuum chamber at 0.2–0.3 Torr. The nozzle temperature was 105 °C and the liquid pressure was about 3.5 bar. Mass spectra were measured for the aqueous solutions with solute molar fractions ($x$) of 0.005, 0.01, 0.02, and 0.038 at an electron energy of 40 eV. Two typical mass spectra are shown in Figure 7. Although the intensities of pure water clusters are nearly the same in most mass spectra of aqueous solutions, the intensities of solute clusters, $AW_n$ and $A_2W_n$ (A = solute and W = $H_2O$), changed depending on the hydrogen-bonding character of the solute molecules. In Figure 7, one can see that the intensities of $H^+$-$CH_3COOH(H_2O)_n$ and $H^+(CH_3COOH)_2(H_2O)_n$ ions are stronger than those of the corresponding monomer and dimer hydrate clusters of $CH_3OH$ appearing in the top spectrum. All of the cluster ions observed for the 13 solute molecules are protonated.

The spectra of the alcohol or carboxylic acid solutions with a solute molar fraction of 0.02 were more complicated due to the contribution of trimer and tetramer hydrate clusters, while even at that solute concentration, amines, acetonitrile, and acetone did not show any trimer hydrate clusters.

**Effect of Cluster Beam Collision with Surrounding Gaseous Molecules on the Observed Distribution of Cluster Ions.** In the early stage of this study, we were afraid that the composition of the clusters might change by the collision of the beams with

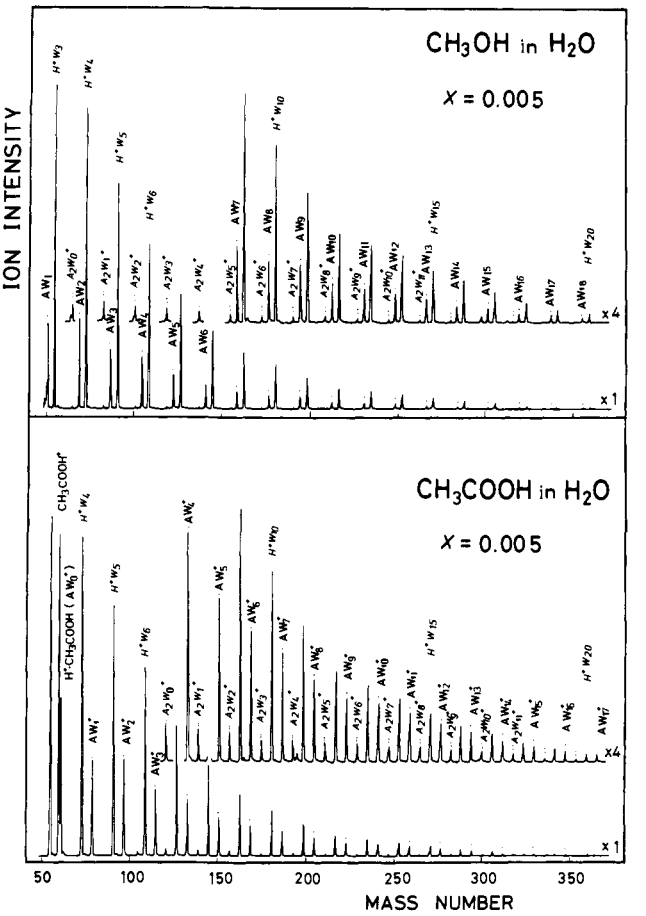


Figure 7. Mass spectra of the cluster beams generated from aqueous methanol solution ($x$ = 0.005, top), and from aqueous acetic acid solution ($x$ = 0.005, bottom). $H^+W_n \equiv H^+(H_2O)_n$, and $AW_n \equiv H^+A(H_2O)_n$. Electron energy = 40 eV.

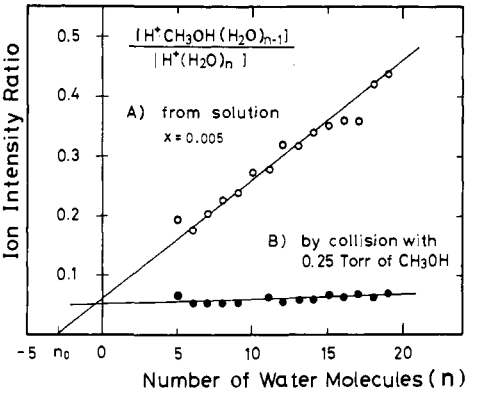


Figure 8. Plots of ion intensity ratios $[H^+CH_3OH(H_2O)_{n-1}]/[H^+(H_2O)_n]$ as a function of $n$. (A) ○, ratios of the cluster ions produced from aqueous solution of methanol with $x$ = 0.005; (B) ●, ratios obtained for the water cluster beam which sustained collision with 0.25 Torr of $CH_3OH$ in the first expansion chamber.

monomer molecules around the beam. To check the collisional effect on the distribution of the clusters, gaseous methanol was introduced in the first (expansion) chamber, thus increasing the pressure up to 0.25 Torr. A pure-water cluster beam produced by the expansion came into collision with methanol gas. This process may attach a methanol molecule to the water clusters but it may also release a water molecule due to the excess energy supplied by the collision. Although the efficiency of this "three-body" process may not be so high, the distribution of $CH_3OH(H_2O)_n$ as a function of the cluster size $n$ is expected to be in proportion to the distribution of the water clusters in the original beam. In fact, the observed intensity ratios $[H^+$-

(12) De Raedt, B.; Sprik, M.; Klein, M. L. *J. Chem. Phys.* **1984**, *80*, 5719.
(13) Hermann, V.; Kay, B. D.; Castleman, A. W., Jr. *Chem. Phys.* **1982**, *72*, 185.

$CH_3OH\cdot(H_2O)_{n-1}]/[H^+(H_2O)_n]$ were nearly constant for the change of the number of water molecules $n$ in the clusters as shown in Figure 8.

In marked contrast to this change, the intensity ratios of the clusters produced from the aqueous solution containing methanol increased linearly with increasing cluster size. Clearly the collisionally generated binary clusters showed different mass-spectral patterns, compared with those produced from the aqueous solution. Most of the spectra obtained with the nozle–skimmer distances shorter than 3 mm were found to have little effect of collision.

Now comes the question why does the intensity ratio increase as the cluster size becomes larger?

**Stochastic Solute Concentration in Clusters.** Fragmentation of a liquid by adiabatic expansion in a vacuum produces clusters with varied sizes and composition. If the intermolecular interaction in the liquid is equivalent for all pairs, a stochastic distribution of solute and solvent molecules in clusters is expected. Consider a droplet with a total number of molecules, $M$, a number of solute molecules, $R$, and a number of solvent molecules, $N$. When a cluster of $m$ molecules is extracted randomly from the droplet, the probability, $P(m,r;M,R)$, that $r$ molecules in the cluster are solute species is given by the following equation

$$P(m,r;M,R) = {}_RC_{r\,N}C_n/{}_MC_m = \frac{R!}{r!(R-r)!}\frac{N!}{n!(N-n)!}\Big/\frac{M!}{m!(M-m)!} \quad (1)$$

where ${}_iC_j$ is a binomial coefficient, $N = M - R$, and $n = m - r$. Since the present experiment produces clusters of a size considerably smaller than droplet size (namely, $M \gg m$, and $R \gg r$), the distribution function can be written as follows

$$P(m,r;M,R) = \frac{m!}{r!(m-r)!}\left(\frac{R}{M}\right)^r\left(\frac{N}{M}\right)^n \quad (2)$$

This function gives a distribution of clusters with $r$ solute molecule(s) in a total number of $m$ molecules. For convenience' sake, such a cluster with $n$ solvent molecules ($n = m - r$) is denoted as an "$r - n$ cluster". Now, we compare the population of an $r - n$ cluster species with that of an $(r + 1) - (n - 1)$ species, where both clusters have the same number of total molecules, $m$

$$\frac{P(m,r+1;M,R)}{P(m,r;M,R)} = \frac{n}{r+1}\frac{R}{N} = \frac{n}{r+1}\frac{x_1}{x_2} \quad (3)$$

where $x_1$ and $x_2$ are the mole fractions of solute and solvent, respectively. This indicates that *the population ratio of the $r - n$ cluster to the $(r + 1) - (n - 1)$ cluster is proportional to the number of solvent molecules ($n$) and the molar ratio of solute to solvent, $x_1/x_2$.*

**Loss of Molecules from Clusters on Electron Impact Ionization.** Electron impact ionization of water clusters is accompanied by a proton-transfer reaction and a fragmentation process

$$(H_2O)_n \xrightarrow{e^-} [(H_2O)_n^+]^* \quad (4)$$

$$[(H_2O)_n^+]^* \rightarrow [(H_2O)_{n-1}H^+]^* + OH \quad (5)$$

$$[(H_2O)_{n-1}H^+]^* \rightarrow (H_2O)_{n-1-s}H^+ + s(H_2O) \quad (6)$$

where * indicates a hot cluster state. For convenience, we set $n' = n - 1 - s$, that is the number of water molecules in an ion cluster. Reaction 5 is a proton-transfer reaction and process 6 is the evaporation of weakly bound molecule(s) from the hot ion cluster. Reactions 4 and 5 take place in a time shorter than 10 ns, whereas reaction 6 takes roughly $10^{-5}$ s.[14] Klots investigated the evaporative cooling of water cluster ions in process 6 theoretically and estimated that at 31 $\mu$s after ionization 28% of the original population will have decayed by evaporating a water molecule.[15] There is no conclusive experimental evidence on the size of $s$ (the number of evaporated water molecule(s)). However, there are some experimental clues that suggest a rough size. (1) The mass spectrum of water clusters at 40 eV shows little change compared to that at 20 eV in a range of water 6-mer to 20-mer suggesting that the primary process of the ionization of clusters is the electronic excitation to states located lower than 20 eV. (2) According to the photoelectron studies of water, a 20 eV electron can remove an electron in nonbonding orbitals ($1b_1$ or $3a_1$).[16,17] In water clusters, these nonbonding orbitals are stabilized due to hydrogen bonding except those of water molecules at edge sites or those of weakly bound molecules at the surface of a cage, in which one nonbonding orbital is really nonbonded and has a much higher orbital energy. The ionization probability of such an edge molecule must be relatively large since the Franck–Condon factor for the ionization of a hydrogen-bonded electron is expected to be smaller than that of an nonbonded electron due to large geometrical change of the hydrogen-bonded pair in the ionized state. If this is the case, ionization is localized around the edge molecule and fragmentation may take place almost independent of cluster size, particularly in large clusters. (3) Direct ionization of hydrogen-bonded electrons by optical excitation of methylamine–water and *N*-methylformamide–water clusters provided much smaller cluster ions compared with the ions generated by electron impact at 20 eV.[18] This indicates that the direct ionization of a hydrogen-bonded electron of a solute molecule cleaves a cluster more drastically than the ionization induced by electron impact. (4) Recent reflectron studies of thermal dissociation of hot clusters of water[14] and ammonia[19] revealed that in the collisionless condition hot clusters mostly evaporate one or two monomer(s).

Thus, we introduce the assumption that the electron impact ionization of hydrate clusters accompanies the evaporation of a small number of water molecules nearly independently of the size of the parent clusters. The validity of this assumption will be discussed in a later section.

**Cluster Ion Intensity Ratios and Stability of Hydrate Clusters.** Clusters that exist in a liquid change their shape, size, and component molecules in a time domain of molecular motion. However, sampling of a large ensemble may give an average distribution of cluster size. Freezing of the clusters is expected to be induced by the evaporation of the molecules weakly bound to the clusters (by van der Waals forces) in an expansion time scale of $10^{-11}$ s for a flight of 100 Å. This estimation is based on the statistical partitioning of the thermal energy to the translational motion of the dissociating fragment. Namely $E_T = kT$. This expansion process is thought to be accompanied by collisional evaporation of molecule(s) from clusters. As revealed by the flow rate dependence (molecular beam density change) and by the outer gas pressure dependence experiments, such collisional processes, however, were found not to change the spectral pattern under the present expansion condition. Change of the spectral pattern was seen when the temperature of the liquid was raised or lowered. Three-body collisions producing larger clusters in the course of the expansion were judged to be negligible due to the pressure in the expansion chamber (0.2–0.3 Torr) and the nozzle–skimmer distance (typically 2.5 mm).

As for the hydrate clusters with a large number of water molecules, evaporation and fragmentation of solute hydrates in the ionizer are considered in the following discussion. In general, one can write the following:

$$\frac{[H^+A(H_2O)_{n'-1}]}{[H^+(H_2O)_{n'}]} = \frac{[A(H_2O)_{n'+t}]}{[(H_2O)_{n'+s+1}]} \quad (7)$$

and

$$\frac{[H^+A_2(H_2O)_{n'-1}]}{[H^+A(H_2O)_{n'}]} = \frac{[A_2(H_2O)_{n'+t}]}{[A(H_2O)_{n'+s+1}]} \quad (8)$$

(14) Echt, O.; Kreisle, D.; Knapp, M.; Recknagel, E. *Chem. Phys. Lett.* **1984**, *108*, 401.
(15) Klots, C. E. *J. Chem. Phys.* **1985**, *83*, 5854.
(16) Brundle, C. R.; Turner, D. W. *Proc. R. Soc. London* **1968**, *A307*, 27.
(17) Kimura, K.; Katsumata, S.; Achiba, Y.; Yamazaki, T.; Iwata, S. *Handbook of HeI Photoelectron spectra of Fundamental Organic Molecules*; Japan Scientific Society Press: Tokyo, 1981; p 33.
(18) Nishi, N.; Shinohara, H.; Yamamoto, K.; Nagashima, U.; Washida, N. *Faraday Discuss. Chem. Soc.* **1986**, *82*, 359.
(19) Echt, O.; Morgan, S.; Dao, P. D.; Stanley, R. J.; Castleman, A. W., Jr. *Proceedings of the 4th Symposium on Atomic and Surface Physics*, Maria Alm, Austria, 1984; p 246.

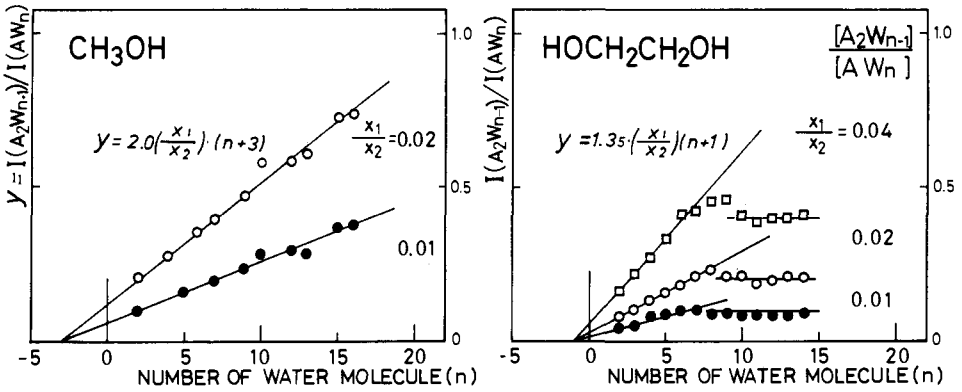


**Figure 9.** Plots of intensity ratios of dimer hydrates ($H^+A_2(H_2O)_{n-1}$) to monomer hydrates ($H^+A(H_2O)_n$) as a function of the number of water molecules ($n$) observed in methanol–water solution ($x_1/x_2 = 0.02$ (○) and 0.01 (●), and in ethylene glycol–water solution ($x_1/x_2 = 0.04$ (□), 0.02 (○), and 0.01 (●)). Solid lines are the best fit to the observed ratios and are expressed by the equations given in the figure.

Under the assumption presented above, $s = t$. At this stage, it is not clear that $s$ or $t$ is a single number or if it is an average number of fragmented monomers. The relation of $s = t$ is a good approximation only for a large $n'$ as discussed above. For relatively small $n'$, $s \neq t$ and we have to consider other combinations of parent clusters based on the stochastic model given by eq 2. One can get the following equations for $\Delta n = \pm 1$ and $\pm 2$.

$$\frac{P(m+1,r+1;M,R)}{P(m,r;M,R)} = \frac{m+1}{r+1}\frac{R}{M} = \frac{n+r+1}{r+1}\frac{x_1}{x_1+x_2} \quad (9)$$

$$\frac{P(m-1,r+1;M,R)}{P(m,r;M,R)} = \frac{n(n-1)}{(r+1)(r+n)}\frac{x_1(x_1+x_2)}{x_2^2} \quad (10)$$

$$\frac{P(m+2,r+1;M,R)}{P(m,r;M,R)} = \frac{(r+n+2)(r+n+1)}{(r+1)(n+1)}\frac{x_1x_2}{(x_1+x_2)^2} \quad (11)$$

and

$$\frac{P(m-2,r+1;M,R)}{P(m,r;M,R)} = \frac{n(n-1)(n-2)}{(r+1)(r+n)(r+n-1)}\frac{x_1(x_1+x_2)^2}{x_2^3} \quad (12)$$

Under the present conditions, $x_1 \ll x_2$ and $r = 0$ and 1. One can see that for $n \geq 10$, all of the above four equations are approximated as follows

$$\frac{P(m',r+1;M,R)}{P(m,r;M,R)} \simeq \frac{n}{(r+1)}\frac{x_1}{x_2} \quad (13)$$

where $m' = m \pm 1$ or $m \pm 2$. The right-hand side is exactly the same as eq 3. Equations 10–12 indicate how the intensity ratios of eq 7 and 8 lose linearity at small solvent numbers in the plots as functions of $n'$ (=number of solvent molecules). Equations 11 and 12 indicate that the ratio of a parent cluster (with total molecules $m$) to that with $m-2$ molecules becomes larger than that expected by eq 3 while the ratio to the parent clusters with two excess molecules ($m+2$) becomes smaller than the value predicted by eq 3. The latter case produces the deviation of the intensity ratio to a lower value. This deviation was actually seen in a formic acid–water system for water numbers smaller than 10.

Figure 9 shows two examples of the plots of the ion intensity ratio, $[H^+A_2(H_2O)_{n'-1}]/[H^+A(H_2O)_{n'}]$ ($\equiv[A_2W_{n-1}]/[AW_n]$), against the number of solvent molecules ($n'$). As predicted by eq 3, the intensity ratio linearly increased as a function of $n'$ and the mole fraction ratio of solute to solvent ($x_1/x_2$). Amazingly, the methanol–water system showed a very nice fit to a line originating at $n' = -3$ in the region of $2 \leq n' \leq 16$. The plots of $[H^+A(H_2O)_{n'-1}]/[H^+(H_2O)_{n'}]$ in Figure 8 also showed a nice fit to a line with the same origin ($n' = -3$). This indicates the validity of eq 8 with the condition of $s = t$. However, this was not always the case. Amines, carboxylic acids, and amides showed deviation from linearity for $n' \leq 4$. Among the 13 solute species, 10 solute molecules showed a linear increment from water 6-mer but the intensity ratio of a dimer hydrate to a monomer hydrate for ethylene glycol and *N*-methylacetoamide was independent of the water number $n'$ in the ranges of $n' \geq 9$ and 6, respectively. At the moment we shall take the major case into account.

Figure 10 shows the plots of the intensity ratio of a monomer hydrate ion to the same size water cluster ion as well as the ratio of a dimer hydrate ion to the same size monomer–hydrate ion (as functions of the number of water molecules) in the systems with acetic acid, isopropyl alcohol, ethylamine, and formamide. In each system, those ratios for very small clusters ($n' \leq 4$) became larger than the values expected from the lines extrapolated from the large cluster region so that their values were omitted in the plots to avoid complexity of the figures. This deviation is thought to originate from the difference in the number of lost molecules. Figure 10 shows two interesting features: (1) the slope of the line connecting the monomer/pure-water or dimer/monomer (hydrated ion) intensity ratios changes with hydrogen-bonding character of the systems, and (2) in each system, the origin of the monomer/pure-water line coincides with that of the dimer/monomer line at a negative value. In relation to 1, we must note that the slope value predicted by eq 3 is $(r+1)^{-1}(x_1/x_2)$. For the monomer/pure-water ratios, this is $1.0(x_1/x_2)$, and for the dimer/monomer ratios $0.5(x_1/x_2)$. These values mean equivalent interactions among any solute or solvent (water) molecules. Since much stronger interaction between a solute and water molecules produces stronger hydrate clusters, those ion intensity ratios are expected to become larger. Here, we introduce the constants $\kappa_1$ and $\kappa_2$, denoting the following quantities that correspond to the slopes of the intensity ratios of monomer hydrate/pure-water cluster and dimer hydrate/monomer hydrate cluster, respectively, in the plots against the number of solvent molecules. Namely,

$$\kappa_1 = \frac{[H^+A(H_2O)_{n'-1}]}{[H^+(H_2O)_{n'}]}\frac{1}{(n'-n_0)}\frac{x_2}{x_1} \quad (14)$$

$$\kappa_2 = 2\frac{[H^+A_2(H_2O)_{n'-1}]}{[H^+A(H_2O)_{n'}]}\frac{1}{(n'-n_0)}\frac{x_2}{x_1} \quad (15)$$

where $n_0$ is the origin of a line, and in most cases $n_0$ is negative. A factor of 2 in the definition of $\kappa_2$ is introduced for the correction by the factor $(r+1)^{-1}$ in eq 3, so that in the stochastic limit both $\kappa_1$ and $\kappa_2$ are 1.0. In a later section, these constants are shown to be related to the equilibrium constants of molecular exchange processes of the clusters.

Listed in Table I are the values of $\kappa_1$ and $\kappa_2$ obtained for 13 aqueous solution systems at a liquid temperature of 65 ± 5 °C and a liquid pressure of 3.0 bar. The highest stability of a monomer hydrate cluster is seen for formic acid which also shows the highest stability of the dimer hydrate. Among alcohol molecules, $\kappa_1$ and $\kappa_2$ of ethanol and isopropyl alcohol are relatively large and the $\kappa_2$ values are comparable to that of formic acid. In contrast with the case of methanol and ethanol, both methylamine

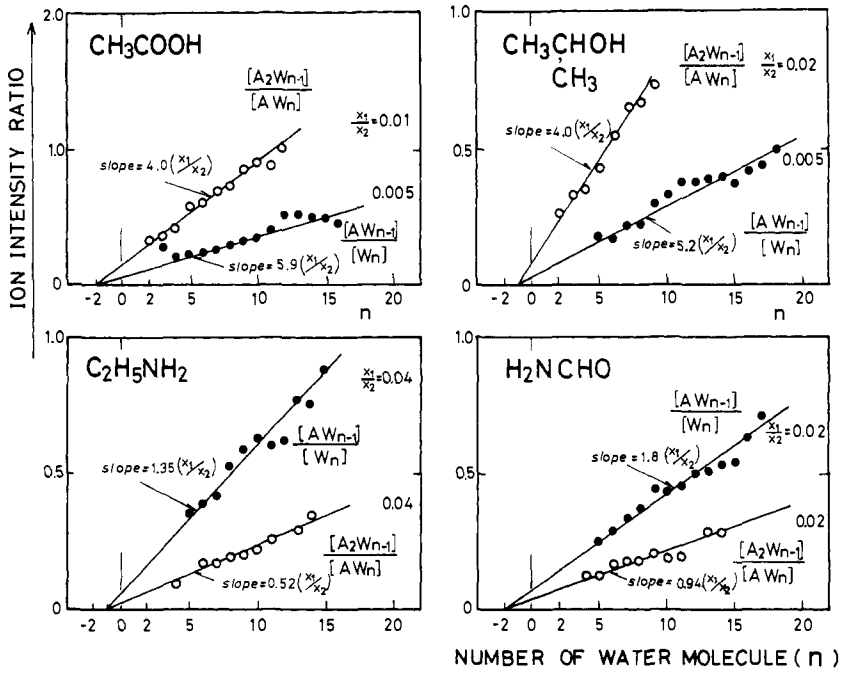


**Figure 10.** Plots of intensity ratios of dimer hydrates to monomer hydrates ($[H^+A_2(H_2O)_{n-1}]/[H^+A(H_2O)_n]$: open circle) and the ratios of monomer hydrates to water clusters ($[H^+A(H_2O)_{n-1}]/[H^+(H_2O)_n]$: filled circle). The slope values of the best fit lines are indicated and the slope is a function of the mole fraction ratio of solute to solvent ($x_1/x_2$).

**Table I** Stability of Monomer Hydrate Clusters and Dimer Hydrate Clusters in Aqueous Solutions Represented As Observed Abundances of the Respective Hydrate Clusters Relative to Stochastic Abundance Expected[a]

| solute species | $\kappa_1$[e] | $\kappa_2$[f] | cluster size valid for $\kappa_1$ | $n_0$ |
|---|---|---|---|---|
| $CH_3OH$ | 4.0 | 4.0 | $4 \le n \le 19$ | −3 |
| $C_2H_5OH$ | 5.3 | 8.4 | $4 \le n \le 13$ | −1 |
| iso-$C_3H_7OH$ | 5.2 | 8.0 | $2 \le n \le 14$ | −1 |
| $HOCH_2CH_2OH$ | 1.6 | 2.7 | $2 \le n \le 8$ | −1 |
| HCOOH | 7.5[b] | 8.4[c] | $14 \le n \le 18$ | −2 |
| $CH_3COOH$ | 5.9 | 8.0 | $4 \le n \le 10$ | −2 |
| $CH_3NH_2$ | 1.3 | 0.9 | $5 \le n \le 14$ | −1 |
| $C_2H_5NH_2$[d] | 1.4 | 1.0 | $5 \le n \le 14$ | −1 |
| $H_2NCHO$[d] | 1.8 | 1.9 | $5 \le n \le 14$ | −2 |
| $CH_3NHCHO$ | 1.3 | 1.6 | $5 \le n \le 11$ | −2 |
| $CH_3NHCOCH_3$ | 0.5 | | $5 \le n \le 15$ | −2 |
| $CH_3CN$ | 0.003 | | $6 \le n \le 20$ | −1 |
| $CH_3COCH_3$ | 0.19 | | $9 \le n \le 19$ | −1 |
| stochastic model | 1.0 | 1.0 | | −1 |

[a] The solutions are at 65 °C under a pressure of 3.0 bar. Definitions of $\kappa_1$, $\kappa_2$, and $n_0$ are given by eq 14 and 15 in the text. [b] The approximation of $s = t$ in eq 7 is only valid for $n > 13$. [c] The approximation of $s = t$ in eq 8 is not valid. Most likely $s = t - 2$. [d] In $D_2O$ solution. [e] Stability of monomer hydrates. [f] Stability of dimer hydrates.

and ethylamine showed $\kappa_1$ and $\kappa_2$ close to the values predicted by the stochastic model, which suggests that the stability of these amine hydrates is comparable to that of pure-water clusters in the solution. This is also seen for $\kappa_1$ of *N*-methylformamide, while the $\kappa_2$ values of formamide and *N*-methylformamide are almost twice as large as those of the amines. The stability of the formamide dimer hydrates is relatively high. Acetonitrile forms very weak hydrate clusters as seen from the value of $\kappa_1$ (=0.003), which is much smaller than that of acetone ($\kappa_1$ = 0.19).

**Number of Evaporated Molecules.** Figures 9 and 10 show the shift of the origins of the lines to a negative integer ($n_0$). In the case of methanol, $n_0 = -3$. This shift is reasonably well understood since the ionization removes some water molecules from the clusters and we have the relations given in (7) and (8). The observed solvation numbers are smaller than those of the parent neutral clusters. Linearity of the intensity ratios holds for the number of solvent molecules or for the total number of molecules of parent clusters as shown in eq 3 or eq 9, respectively. Plots against the number of solvent molecules of the ions caused a shift of the origins to the negative side in most cases. Equation 3 or eq 9 suggests that $n_0$ is related to the number of evaporated molecules ($s + 1$).

**Relation of $\kappa_1$ and $\kappa_2$ to Equilibrium Constants.** Stability of solute–solvent clusters may be expressed by the equilibrium constants of the following "molecular exchange reactions"

$$(H_2O)_n + A \xrightarrow{K_1^n} A(H_2O)_{n-1} + H_2O \tag{16}$$

$$A(H_2O)_n + A \xrightarrow{K_2^n} A_2(H_2O)_{n-1} + H_2O \tag{17}$$

where

$$K_1^n = \frac{[A(H_2O)_{n-1}][H_2O]}{[H_2O]_n[A]} = \frac{[A(H_2O)_{n-1}]}{[(H_2O)_n]}\frac{x_2}{x_1} \tag{18}$$

$$K_2^n = \frac{[A_2(H_2O)_{n-1}][H_2O]}{[A(H_2O)_n][A]} = \frac{[A_2(H_2O)_{n-1}]}{[A(H_2O)_n]}\frac{x_2}{x_1} \tag{19}$$

By combining eq 7, 8, 14, 15, 18, and 19, one can obtain the following relationships for large hydrate clusters

$$\kappa_1 = K_1^n/n \tag{20}$$

and

$$\kappa_2 = 2K_2^n/n \tag{21}$$

where $n = n' - n_0$ and the range of $n'$ is limited as listed in Table I. In this range, $\kappa_1$ and $\kappa_2$ are independent of the cluster size, while $K_1^n$ and $K_2^n$ are proportional to the number of water molecules ($n$) in the clusters. Thus it becomes much clearer that $\kappa_1$ and $\kappa_2$ are general parameters that describe the stability of monomer hydrates and dimer hydrates in aqueous solution, respectively.

As long as the linearity of the intensity-ratio plot is maintained and the observed value of $n_0$ is negative, the condition of $s = t$ in eq 7, 8, 20, and 21 must hold. Even for $s = t - 1$, $\kappa_1$ and $\kappa_2$ are nearly proportional to $K_1^n$ and $K_2^n$. Thus the definition of the stability constants by eq 14 and 15 is convenient and well suited to describing the relative stability of hydrate clusters.

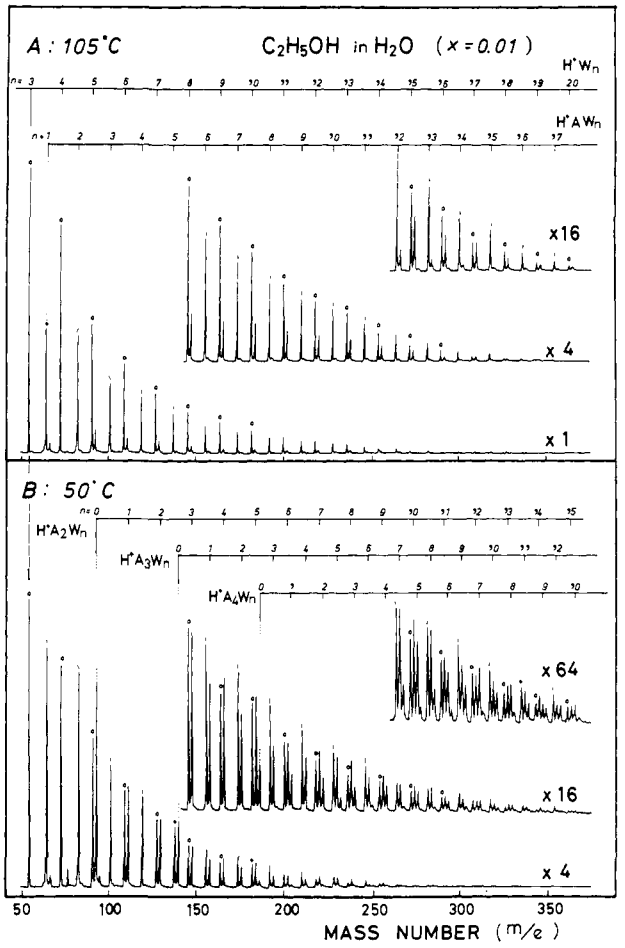


**Figure 11.** Mass spectra of the cluster beams generated from an aqueous ethanol solution ($x$ = 0.01) at 105 °C (A) and 50 °C (B): (0) $H^+(H_2O)_n$, (1) $H^+A(H_2O)_n$ (A = $C_2H_5OH$). Electron energy = 40 eV.

**Temperature Dependence of Intensity Ratios and Van't Hoff Plots.** All of the systems investigated showed spectral changes with increasing temperature. Here we show one typical example of the ethanol–water system. An aqueous solution of ethanol at a mole fraction of 0.01 produced a cluster distribution that was more complicated at lower temperatures as shown in Figure 11. In the higher temperature spectrum (top), enhancement of monomer hydrate cluster signals was prominent. Apparently, the cluster composition change of the solution is reflected in the spectral pattern.

A cluster composition change is the change in the equilibrium of cluster destruction and evolution processes in a liquid. Let us first consider "reactions" 16 and 17. The free energy change ($\Delta G_i^n$) of such a process is expressed by the following equation[20]

$$\Delta G_i^n = -RT \ln K_i^n = \Delta H_i^n - T\Delta S_i^n \qquad (22)$$

Namely

$$\ln K_i^n = -(\Delta H_i^n/R)(1/T) + \Delta S_i^n/R \qquad (23)$$

where $\Delta H_i^n$ and $\Delta S_i^n$ are the enthalpy change and the entropy change of the exchange reaction, respectively. By using eq 7, 8, 18, and 19, one can rewrite eq 23 as follows

$$\ln \frac{[H^+A_i(H_2O)_{n-s-1}]}{[H^+A_{i-1}(H_2O)_{n-s}]} = -(\Delta H_i^n/R)(1/T) + \Delta S_i^n/R + \ln x_1/x_2 \qquad (24)$$

Thus, the logarithmic plot of the intensity ratio against $T^{-1}$ gives

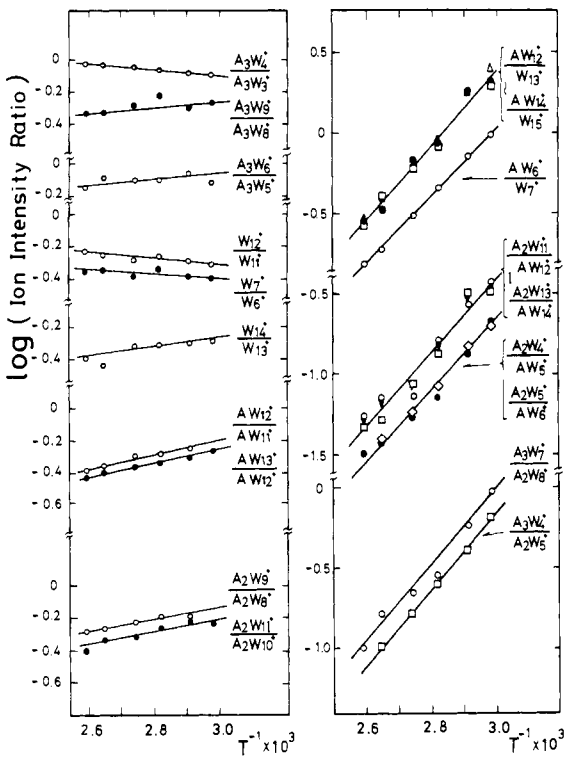


**Figure 12.** Logarithmic plots of intensity ratios $[H^+(C_2H_5OH)_i(H_2O)_{n-1}]/[H^+(C_2H_5OH)_{i-1}(H_2O)_n]$ (right) and $[H^+(C_2H_5OH)_i(H_2O)_{n+1}]/[H^+(C_2H_5OH)_i(H_2O)_n]$ (left) as functions of $1/T$.

the enthalpy and the entropy changes of the exchange process.

For a water attachment process shown by the equation

$$A_i(H_2O)_n + H_2O \xrightarrow{K_{i,w}^{n,1}} A_i(H_2O)_{n+1} \qquad (25)$$

one can obtain the following relationship for the condition of $x_1 \ll 1$.

$$\ln \frac{[A_i(H_2O)_{n+1}]}{[A_i(H_2O)_n]} \propto -(\Delta H_{i,w}^{n,1}/R)(1/T) \qquad (26)$$

On the basis of the assumption that both solute hydrates lose the same number of water molecule(s) on electron impact ionization, the left side of eq 26 is expressed in terms of the fragment ion intensity ratio

$$\ln \frac{[H^+A_i(H_2O)_{n+1-s}]}{[H^+A_i(H_2O)_{n-s}]} \propto -(\Delta H_{i,w}^{n,1}/R)(1/T) \qquad (27)$$

Figure 12 shows the van't Hoff plots of some intensity ratios obtained in the ethanol–water (1:100) system. The intensity ratios changed differently depending on the type of clustering processes. Exchange processes showed a positive slope but the water attachment processes for the water numbers smaller than $9 - m$ ($m$ = solute number) provided negative slopes in the plots against $T^{-1}$. The results of the analysis are summarized in Figure 13 where the enthalpy changes for the processes seen via the fragment-ion intensity changes are shown. Assignment of the parent species is not indicated, but on the basis of the experimental evidence shown in an above section, one can reasonably assume the clusters with one (or two) excess water molecule(s) to be the parent species of the ions.

Figure 13 indicates some interesting features of the solution, but it should not be viewed in a similar way to a gas-phase energy diagram. It is meaningful only when one considers various equilibrium processes of molecular exchange, dissociation, and attachment "reactions". Each $\Delta H$ involves a differentiation step in those equilibrium processes. The actual population in each level is described by a partition function with combination factors of cluster levels and weight factors as functions of molar fractions. In neat liquid water, the enthalpy change on large cluster for-

(20) Murrell, J. N.; Boucher, E. A. *Properties of Liquids and Solutions*; J. Wiley & Sons: New York, 1982; Chapter 10, Section 1.

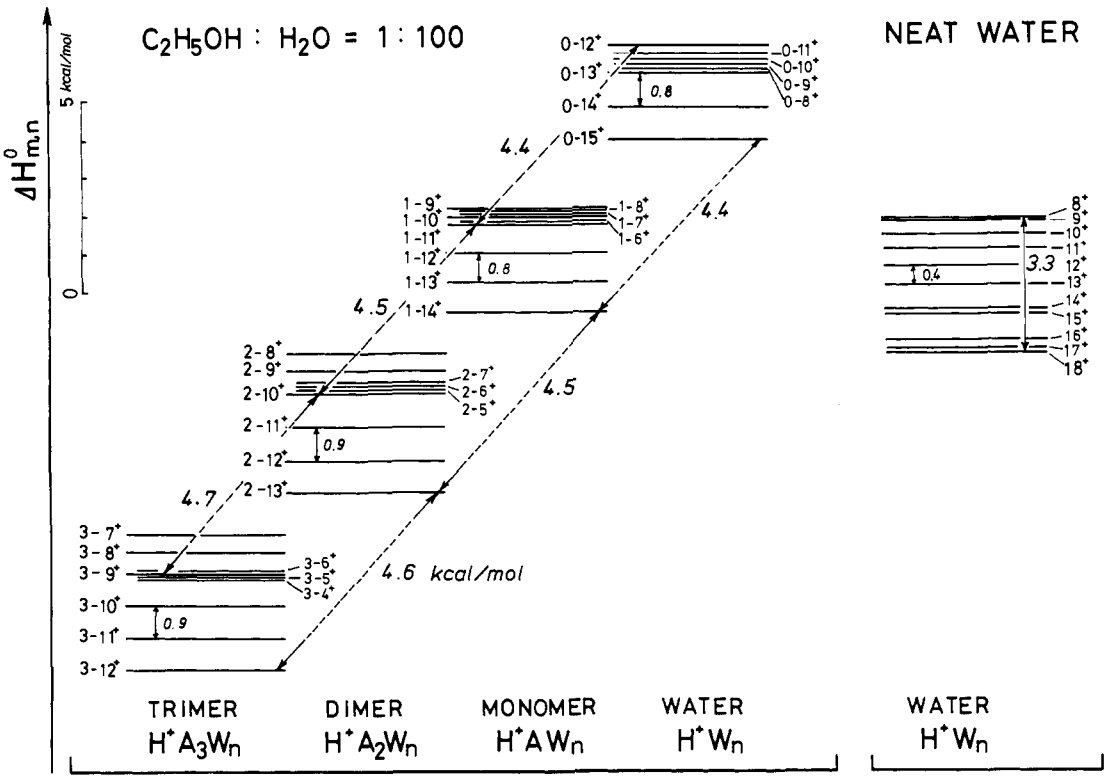


**Figure 13.** Enthalpy changes for molecular exchange processes (eq 16 and 17, shown by dotted arrows) and for water attachment processes (eq 25, solid arrows) in an ethanol–water (1:100) solution under the pressure region of 3.0–3.8 bar. Errors for the respective values are ±0.5 kcal/mol. For comparison, enthalpy changes of water attachment processes are shown with the reliable values marked. Both $m - n^+$ and $H^+A_mW_n$ stand for $H^+(C_2H_5OH)_m(H_2O)_n$, and $n^+$ represents $H^+(H_2O)_n$.

mation becomes lower resulting in the increase of the structural rigidness with decreasing temperature. Addition of 1 mol % ethanol to water (2.6 g of ethanol in 100 g of water) changes the water networks drastically. Exchange of a water for an alcohol is highly preferable so that water molecules tend to form clusters with more alcohol molecules. Frank and Evans[5] stated that microscopic icebergs (formed around nonpolar solute molecules) are also formed about the nonpolar parts of polar molecules such as alcohols and amines. However, the "icebergs", if they exist in the alcohol–water (1:100) system, must have characters different from those present in alkane–water systems, since some water molecules may be bound to alcohol(s) due to hydrogen bonding.

According to ab initio calculations,[21-25] the hydrogen bond energy of alcohol–alcohol dimers is not so different from that of water–water dimers or an alcohol–water hydrogen bond. A very important fact is that the stabilization energies for the addition of one ethanol molecule to pure water clusters, to monomer hydrates, and to dimer hydrates are almost the same (ca. 4.5 + 0.9 kcal/mol). *The observed trend of ethanol–ethanol association is therefore attributed to the hydrophobic hydration of an ethyl group of an ethanol molecule in aqueous environment.* The idea of the "hydrophobic bond" introduced by Kauzmann[24] and Tanford[25] does not explain the observed trend of ethanol–ethanol association in the present diluted solution. In the gas phase, a trans configuration of ethyl groups in an ethanol dimer is most stable.[26] In aqueous solution, the ethyl groups will be surrounded by orientationally ordered water molecules accompanied by hydrogen-bonding networks. The "hydrophobic bond" will be seen in the aqueous solution with much more alcohol concentration.

Formation of higher water clusters can be seen only at high temperatures where alcohol polymers dissociate and interactions between clusters decrease. The trend of alcohol "oligomerization" becomes more prominent in higher concentration solutions and the highly interesting results on the concentrated alcohol–water system will be reported in a subsequent paper.

**Acknowledgment.** We thank Dr. K. Koga and Dr. K. Nagami in Suntory Research Institutes and Dr. U. Nagashima and Dr. H. Tanaka in IMS for stimulating discussions. N.N. expresses hearty thanks to the late Prof. T. Fujiyama for his introduction to this study.

**Registry No.** Acetone, 67-64-1; acetonitrile, 75-05-8; methanol, 67-56-1; ethanol, 64-17-5; 2-propanol, 67-63-0; 1,2-ethanediol, 107-21-1; formic acid, 64-18-6; acetic acid, 64-19-7; methylamine, 74-89-5; ethylamine, 75-04-7; formamide, 75-12-7; *N*-methylformamide, 123-39-7; *N*-methylacetamide, 79-16-3.

(21) Tse, Y.-C.; Newton, M. D.; Allen, L. C. *Chem. Phys. Lett.* **1980**, *75*, 350.
(22) Alagona, G.; Tani, A. *J. Chem. Phys.* **1981**, *74*, 3980.
(23) Curtiss, L. A.; Frurip, D. J.; Blander, M. *J. Chem. Phys.* **1981**, *75*, 5900.
(24) Kauzmann, W. *Adv. Protein Chem.* **1959**, *14*, 1.
(25) Tanford, C. *The Hydrophobic Effect—Formation of Micelles and Biological Membranes*; Wiley-Interscience: New York, 1973.
(26) Nagashima, N., private communication on a geometry optimized 6-31G** calculation of ethanol–ethanol, ethanol–water, and water–water complexes.